Articles

Implications for Viral Capsid Assembly from Crystal Structures of HIV-1 Gag_{1-278} and $CA^{N}_{133-278}$[†,‡]

Brian N. Kelly,[§] Bruce R. Howard,[⊥] Hui Wang,[§] Howard Robinson,[∥] Wesley I. Sundquist,*[,§] and Christopher P. Hill*[,§]

Department of Biochemistry, University of Utah, Salt Lake City, Utah 84112-5650, and Department of Biology, Brookhaven National Laboratory, Upton, New York 11973-5000

Received May 10, 2006; Revised Manuscript Received July 18, 2006

ABSTRACT: Gag, the major structural protein of retroviruses such as HIV-1, comprises a series of domains connected by flexible linkers. These domains drive viral assembly by mediating multiple interactions between adjacent Gag molecules and by binding to viral genomic RNA and host cell membranes. Upon viral budding, Gag is processed by the viral protease to liberate distinct domains as separate proteins. The first two regions of Gag are MA, a membrane-binding module, and CA, which is a two-domain protein that makes important Gag−Gag interactions, forms the cone-shaped outer shell of the core (the capsid) in the mature HIV-1 particle, and makes an important interaction with the cellular protein cyclophilin A (CypA). Here, we report crystal structures of the mature CA *N*-terminal domain ($CA^{N}_{133-278}$) and a MA−CA^{N} fusion (Gag_{1-278}) at resolutions/R_{free} values of 1.9 Å/25.7% and 2.2 Å/25.8%, respectively. Consistent with earlier studies, a comparison of these structures indicates that processing at the MA−CA junction causes CA to adopt an *N*-terminal β-hairpin conformation that seems to be required for capsid morphology and viral infectivity. In contrast with an NMR study (Tang, C., et al. (2002) *Nat. Struct. Biol. 9,* 537−543), structural overlap reveals only small relative displacements for helix 6, which is located between the β-hairpin and the CypA-binding loop. These observations argue against the proposal that CypA binding is coupled with β-hairpin formation and support an earlier surface plasmon resonance study (Yoo, S., et al. (1997) *J. Mol. Biol. 269,* 780−795), which concluded that β-hairpin formation and CypA-binding are energetically independent events.

Assembly of HIV particles is driven by the Gag polyprotein, which is the major viral structural protein and is present at about 5000 copies per virion (*1*). Gag is comprised of several distinct regions that are processed by the viral protease as virions bud from the host cell, thereby releasing discrete new proteins required for maturation (*2*, *3*). The *N*-terminal 132-residue MA domain confers membrane-binding activity to Gag, and the MA protein (aka p17) remains associated with the viral membrane after processing. Membrane binding is bipartite, with electrostatic interactions made by positively charged MA side chains and hydrophobic interactions provided by the insertion of MA's *N*-terminal myristate moiety into the lipid bilayer (*4*). Several structures of the MA protein have been determined by NMR (*5*, *6*) and X-ray crystallography (*7*, *8*), and they are in good agreement with each other. Although the unmodified HIV-1[1] MA protein is monomeric in solution (*5*), crystal structures of HIV-1 (*7*) and SIV (*8*) MA reveal a trimeric association that may represent the arrangement upon membrane binding and interaction with the trimeric ENV protein (*9*, *10*). NMR and sedimentation analyses of the myristoylated MA protein support this view by revealing that the Myr group can pack into a surface pocket of the MA structure or extrude and enhance trimerization, particularly of longer MA−CA fragments (*6*).

The 231-residue CA region immediately follows MA in the HIV-1 Gag polyprotein. The extended Gag molecules adopt a radial distribution in the spherical immature particle, and the CA layer is located ∼100 Å from the membrane (*11*, *12*). During the subsequent process of maturation, ∼1000−1500 CA protein (aka p24) molecules rearrange to form the distinctive conical capsid of infectious virions,

[†] This work was supported by the NIH (Grant AI 45405 to W.I.S. and C.P.H.) and the Offices of Biological and Environmental Research and of Basic Energy Sciences of the U.S. Department of Energy/National Center for Research Resources of the NIH.

[‡] Coordinates and structure factors have been deposited in the Protein Data Bank with accession codes 2GOL (Gag_{1-278}) and 2GON ($CA^{N}_{133-278}$).

* To whom correspondence should be addressed. Tel: 801-585-5402. Fax: 801-581-7959. E-mail: wes@biochem.utah.edu (W.I.S.). Tel: 801-585-5536. Fax: 801-581-7959. E-mail: chris@biochem.utah.edu (C.P.H.).

[§] University of Utah.

[∥] Brookhaven National Laboratory.

[⊥] Present address: Department of Physical Science, Southern Utah University, Cedar City, UT 84720.

[1] Abbreviations: HIV-1, human immunodeficiency virus type 1; CypA, Cyclophilin A.

10.1021/bi060927x CCC: $33.50
Published on Web 09/01/2006

which is organized as a fullerene cone (*13*−*15*). The CA protein is comprised of two domains (*16*). The *N*-terminal domain ($CA^N_{133-278}$; Gag residues 133−278) mediates hexamer formation in the viral capsid, and the *C*-terminal domain (CA^C: Gag residues 279−363) mediates CA dimerization in solution and association of adjacent CA hexamers in the core (*14*, *17*). A detailed model for the CA^N hexamer is provided by the crystal structure of the CA^N protein of murine leukemia virus (MLV) (*18*). This structure is consistent with earlier EM reconstructions of the HIV-1 CA hexamer (*14*) and reveals relatively polar intersubunit interactions mediated by CA^N helices 1, 2, and 3. A detailed model of the mature CA CTD dimer is provided by crystal structures (*17*, *19*). A related but domain-swapped dimer model has been proposed for the immature CA CTD by analogy with the structurally related SCAN domain (*20*). Finally, an additional site of contact between the *N*- and *C*-terminal domains is supported by biochemical studies (*21*) but has not yet been visualized at high resolution.

Following Gag proteolysis, the *N*-terminal residues of $CA^N_{133-278}$ adopt a β-hairpin conformation that is stabilized by a salt bridge between Asp183 (Gag numbering is used throughout) and the free cationic CA^N *N*-terminal amine (*16*). Stabilization of the β-hairpin conformation by the free CA^N *N*-terminus means that its formation is favored by Gag processing. β-hairpin formation appears to be important for viral maturation and assembly of the conical capsid (*22*, *23*), although its precise role remains unclear.

Another important role of CA^N is to bind the cellular protein cyclophilin A (CypA) (*24*). This interaction plays an important role in HIV-1 infectivity, probably because CA−CypA interactions within the target host cell modulate the binding of host restriction factors (*25*−*29*). The CypA active sites bind the Gly221-Pro222 dipeptide (*30*−*32*), which is located on an inherently flexible 18-residue cyclophilin-binding loop. HIV-1 CA is a substrate for CypA-catalyzed proline isomerization (*33*), although it is not yet known if the CypA rotamase activity is important for HIV-1 infectivity. CA/CypA complexes in which the Gly221-Pro222 peptide adopts either cis or trans conformation have been visualized in a series of crystal structures, which indicate that the cis−trans isomerization activity of CypA proceeds by rotation of residues *N*-terminal to the bound proline (*34*). An alternative mechanism of *C*-terminal rotation has also been proposed (*35*).

In order to extend our understanding of the structural basis for HIV assembly and maturation, we have determined the crystal structures of Gag_{1-278} (i.e., the fused MA and CA^N domains) at 2.2 Å resolution and the free $CA^N_{133-278}$ domain (A224E mutant) at 1.9 Å resolution. A key finding is that the structure of CA remains largely unchanged upon proteolysis at the MA−CA junction, with the exception of β-hairpin formation in the $CA^N_{133-278}$ structure. This observation indicates that CypA binding is unlikely to be significantly affected by Gag processing and is consistent with the view that conformational changes that allow the formation of the conical viral core are likely to be centered on the β-hairpin and residues near the *N*-terminus of helix 1.

MATERIALS AND METHODS

$CA^N_{133-278}$ Expression and Purification. Native CA^N(A224E) protein ($CA^N_{133-278}$) was expressed in *E. coli* BL21(DE3) at 23 °C. Protein expression was induced at an optical density (A_{600}) of ∼0.7 with 1 mM IPTG. All subsequent steps were performed at 4 °C. Cells were harvested 4 h post induction by centrifugation, lysed in a French press, and sonicated to reduce viscosity. Insoluble material was removed by centrifugation at 25 900*g* for 50 min, and the crude $CA^N_{133-278}$ protein was precipitated by the addition of 0.4 equiv of saturated $(NH_4)_2SO_4$ solution. The pellet was dissolved in a buffer of 25 mM Tris-HCl (pH 8.0) and 5 mM β-mercaptoethanol, and chromatographed on a Q-Sepharose column (Pharmacia). The protein eluted at ∼300 mM NaCl using a linear gradient from 0 to 1 M NaCl in 25 mM Tris-HCl (pH 8.0) and 5 mM β-mercaptoethanol. Fractions containing the protein were pooled, dialyzed in 25 mM 4-morpholinepropanesulfonic acid potassium salt (KMOPS) at pH 6.8, 1 M $(NH_4)_2SO_4$, 5 mM β-mercaptoethanol, and loaded onto a Phenyl Sepharose column (Pharmacia). $CA^N_{133-278}$ was eluted at ∼200 mM $(NH_4)_2SO_4$ using a linear gradient from 1 to 0 M $(NH_4)_2SO_4$ in 5 mM KMOPS at pH 6.8 and 5 mM β-mercaptoethanol. Selenomethionine substituted $CA^N_{133-278}$ was expressed in the methionine auxotroph B834(DE3) in M9 minimal media supplemented with amino acids. IPTG and selenomethionine were added at mid log phase (*36*). This procedure typically yielded 25 mg of pure $CA^N_{133-278}$.

$CA^N_{133-278}$ Structure Determination. Crystals were grown at 13 °C in sitting drops containing a 1:1 mixture of protein solution (1.5 mM $CA^N_{133-278}$, 10 mM Tris-HCl at pH 8.0, and 2 mM β-mercaptoethanol) and reservoir solution (0.2 M biammonium citrate and 20% PEG 3350). Crystals were transferred to light mineral oil followed by removal of all extraneous mother liquor before suspension in a rayon loop and plunging into liquid nitrogen. MAD data were collected from a single crystal of selenomethionine-substituted $CA^N_{133-278}$ and were processed with the HKL suite (*37*). Phases were determined using SOLVE (*38*). Mapfitting and refinement were performed using O (*39*) and REFMAC5 (*40*). Crystallographic statistics are given in Table 1.

Gag_{1-278} Expression and Purification. Gag_{1-278} was expressed with an *N*-terminal extension that includes eight histidine residues and can be removed by the TEV protease to yield residues 1−278 of HIV-1_{NL43} Gag, including the initiator Met1 and preceding non-native glycine and histidine residues. Induction of expression was the same as that for $CA^N_{133-278}$ (above). Cells from 5 L of bacterial culture were resuspended in 45 mL of nickel column lysis buffer (50 mM imidazole, 0.5 M NaCl, and 20 mM Tris at pH 7.4) and incubated on ice for 30 min in the presence of 50 mg of lysozyme and 45 μL of 1000× protease inhibitors (pepstatin, aprotinin, and leupeptin) (Sigma) and 100 μL of PMSF (Research Biochemicals International). Subsequent steps were performed at 4 °C unless otherwise noted. The lysate was sonicated, clarified by centrifugation, and applied to a Ni-NTA agarose column (Qiagen). Washing with three column volumes of lysis buffer made to 80 mM imidazole was followed by elution with five column volumes of lysis buffer made to 500 mM imidazole. Fractions containing Gag_{1-278} were dialyzed into TEV cleavage buffer (50 mM

Table 1: Crystallographic Data and Refinement of $CA^N_{133-278}$[a]

	inflection	peak	high remote
wavelength (Å)	0.97895	0.97858	0.94002
no. of observed reflections	362 801	360 474	663 131
no. of unique reflections	48 627	48 309	48 798
resolution (Å)	40.0−1.90	40.0−1.90	40.0−1.90
highest resolution shell (Å)	1.95−1.90	1.95−1.90	1.95−1.90
completeness (%)	99.5 (100.0)	99.5 (99.9)	99.9 (100.0)
R-sym (%)[b]	7.6 (54.3)	8.4 (50.8)	7.7 (46.1)
average $I/\sigma(I)$	17.1 (3.6)	15.0 (3.9)	34.4 (4.4)
mosaicity (deg)	0.331	0.338	0.347
refinement			
resolution (Å)			19.80−1.90
R factor (%)[c]			20.2
R_{free} (%)[d]			25.7
R overall (%)[e]			20.5
no. of non-hydrogen atoms			4 484
no. of water molecules			226
RMSD bond (Å)[f]			0.024
RMSD angles (deg)			1.78
ϕ/ψ angles for non-Gly/Pro residues			
most favored regions (%)			92.8
additional allowed regions (%)			6.1
generously allowed regions (%)			0.5
disallowed regions (%)			0.7
average *B* factor			
main chain atoms (Å^2)			34
side chain atoms (Å^2)			37
water molecules (Å^2)			38
citrate molecules (Å^2)			36

[a] The space group is $P2_12_12$ and cell dimensions are $a = 106.3$ Å, $b = 134.5$ Å, and $c = 42.1$ Å. The data for $CA^N_{133-278}$ were collected on a Quantum 4 CCD detector at SSRL (Stanford) beamline 9-2. The values in parentheses refer to the high-resolution shell. [b] *R*-sym $= 100 \times \Sigma |(I - \langle I \rangle)|/\Sigma(I)$. [c] *R* factor $= 100 \times \Sigma||Fo| - k|Fc||/|Fo|$ for reflections included in refinement calculations. [d] R_{free} is the *R* factor calculated for data not used in the refinement (5%). [e] *R* overall is the *R* factor calculated using all observed data after a final cycle of refinement. [f] Stereochemical statistics were computed with PROCHECK (*67*).

Tris at pH 8.0, 150 mM NaCl, 5mM EDTA, and 1 mM DTT) followed by overnight incubation with 0.2 mg of TEV protease at 23 °C. The cleaved protein was further purified on an SP column (Amersham Pharmacia Biotech) using a linear gradient from 50 mM to 1 M NaCl in 25 mM MOPS at pH 6.8 and 5 mM β-mercaptoethanol. Gag_{1-278} eluted at approximately 600 mM NaCl. The final purification step was gel filtration chromatography on an SD75 column (Amersham Pharmacia Biotech) in 10 mM Tris at pH 7.4, 100 mM NaCl, and 5 mM β-mercaptoethanol. The protein was concentrated to 0.27 mM for crystal growth. The purified protein was confirmed to be full length Gag_{1-278} by *N*-terminal sequencing (GHMGARA) and mass spectrometry (observed 31206.6 Da, calculated 31207.6 Da). This procedure typically yielded 8 mg of pure Gag_{1-278}. Selenomethionine substituted Gag_{1-278} was expressed using BL21(DE3) cells in M9 minimal media (*41*). Amino acids, including selenomethionine were added at an OD_{600} value of 0.5. The cells were induced with 1 mM IPTG, and protein expression took place for 12 h at 23 °C.

Gag_{1-278} Structure Determination. Gag_{1-278} crystals grew within two weeks in hanging drops at 21 °C. The reservoir solution was 28% PEG 8000, 0.2 M $(NH_4)_2SO_4$, and 0.1 M sodium cacodylate at pH 6.7. The drop was a 1:1 mixture of protein and reservoir solutions. The crystals were transferred for a few seconds to the reservoir solution to which glycerol was added to a final glycerol concentration of 25%, suspended in a rayon loop, and cryocooled by plunging into liquid nitrogen. Data were processed with the HKL suite (*37*).

SOLVE (*42*) was used to locate Se positions from the 3.4 Å resolution SAD data. This allowed positioning of one CA^N domain by the matching of Se sites to the positions of Met residues within the known CA^N structure. Following rigid body refinement, additional CA^N and MA domains were located by molecular replacement using EPMR (*43*). Refinement calculations were performed by REFMAC5 (*40*), operated via the CCP4 interface (*44*). Map fitting was performed using XTALVIEW (*45*). Crystallographic statistics are summarized in Table 2. Figures were made with Pymol (*46*).

RESULTS AND DISCUSSION

Gag_{1-278} Structure Determination. The HIV-1 Gag_{1-278} construct encompasses the entire MA and CA^N domains. It is identical to the Gag_{1-283} construct whose NMR structure was reported earlier (*47*) except that it has two additional residues at the *N*-terminus and lacks five CA residues and a polyhistidine tag at the *C*-terminus (all of which were disordered in the NMR structure).

The Gag_{1-278} structure was determined using SAD data collected from a selenomethionine-substituted crystal. A CA^N domain was docked on the Se positions, and molecular replacement was used with higher quality native data to locate the other CA^N and MA domains. The structure has been refined to an *R* factor (R_{free}) of 0.205 (0.258) against 2.2 Å data and displays good geometry (Table 2). The crystal possesses two Gag_{1-278} molecules per asymmetric unit, although only one of the two MA domains is visible in electron density maps. The possibility of partial proteolysis during crystallization was discounted by SDS−PAGE visualization of washed crystals, which revealed a single species

Table 2: Crystallographic Data and Refinement of Gag_{1-278}[a]

	native	SAD
space group	$P4_12_12$	$P4_12_12$
unit cell dimensions (Å)	a=111.0, c = 113.4	a=111.0, c = 113.1
wavelength (Å)	1.0000	0.97791
resolution (Å) (high)	30.0−2.20 (2.26−2.20)	30.0−3.30 (3.42−3.30)
no. of observed reflections	565,720	94,384
no. of unique reflections	34,399	10,253
completeness (%)	93.9 (73.3)	99.2 (94.1)
R-sym (%)	8.0 (52.4)	11.4 (34.8)
average $I/\sigma(I)$	15 (2)	7 (3.25)
mosaicity (deg)	0.56	0.44
refinement		
R factor (%)	20.25	
R_{free} (%)	25.83	
R overall (%)	20.53	
number of non-hydrogen atoms	3219	
number of water molecules	274	
RMS deviations in bond lengths (Å)	0.025	
bond angles (deg)	2.105	
ϕ/ψ angles for non-Gly/Pro residues		
most favored regions (%)	91.7	
additional allowed regions (%)	7.3	
generously allowed regions (%)	0.6	
disallowed regions (%)	0.3	
average B factors		
main chain atoms (Å^2)	48	
side chain atoms (Å^2)	50	
water molecules (Å^2)	56	

[a] Data for Gag_{1-278} were collected at NSLS (Brookhaven) on beamlines X25 (native) and X12C (SAD) using ADSC Q315 and Q210 CCD detectors, respectively. See Table 1 footnote for definitions.

that comigrated with full length Gag_{1-278} (data not shown). We, therefore, conclude that the missing MA domain is present within the crystal but is mobile and adopts a range of orientations. This is consistent with packing of the crystal lattice, which contains large volumes of bulk solvent that could accommodate an MA domain in a variety of locations. Assuming two full-length Gag_{1-278} molecules per asymmetric unit, the solvent content is estimated to be 56%.

Gag_{1-278} Structure Description. The crystal structure indicates that Gag_{1-278} comprises ordered MA and CA^N domains that are connected by a flexible linker (Figure 1a and b). MA comprises a globular structure of six helices, and CA comprises a helical bundle of four helices (H1, H2, H3, and H7) with H4 packing at an angle that imparts an overall arrowhead shape. The relatively short H5 and H6 helices pack perpendicular to the four helix bundle at the top of the structure. This same arrangement was reported for the structure of Gag_{1-283} determined in solution (*47*), and the MA and CA^N domains of Gag_{1-278} superimpose closely with those of the Gag_{1-283} structure and previously determined structures of the isolated domains.

The 101 ordered residues of the Gag_{1-278} MA domain (Figure 1a) overlap previously determined MA structures (*5*−*7*) with an RMSD on all Cα atoms that ranges between 1.0 and 1.9 Å. The largest deviations are in residues 66−74, a region that adjusts in response to MA trimer formation (*48*). In contrast to previously determined HIV-1 (*7*) and SIV (*8*) MA crystal structures, both of which displayed a trimeric association, the MA domain is monomeric in the Gag_{1-278} crystal. The structure does not suggest a reason why isolated MA protein might trimerize, whereas the MA domain of Gag_{1-278} would be prevented from forming this arrangement. Consistent with NMR data indicating that myristate exposure favors trimerization (*6*), we favor the possibility that the MA protein and the MA domain of Gag trimerize upon binding the membrane. Presumably, the absence of membrane association and myristoylation of Gag_{1-278} allows the crystal packing forces of some lattices to overcome the inherently weak affinity, whereas other lattices accommodate the trimeric state.

The last 25 residues of the Gag_{1-278} MA domain and the first 10 residues of the CA^N domain are disordered and have been omitted from the refined model of Gag_{1-278}. This flexibility for residues 108−143 could easily accommodate the ∼40 Å gap between the MA and CA^N domains that has been inferred for immature virions from electron microscopy (*12*). Indeed, this disorder makes it unclear as to which of the two CA^N domains in the asymmetric unit is attached to the one visible MA domain because the *C*-terminus of the MA domain is sufficiently close to build a hypothetical connection to either of the CA^N domains. This uncertainty does not diminish the interpretation of mechanistic significance because the primary point is that the linker between MA and CA^N domains is highly flexible in Gag. This flexibility may be required to form an extended conformation that is accessible by the HIV-1 protease.

$CA^N_{133-278}$ Structure Determination. The HIV $CA^N{}_{133-278}$ protein (Gag residues 133−278 and CA residues 1−146) was expressed in *E. coli* with the authentic CA *N*-terminus. The sequence corresponds to wild-type HIV-1_{NL4-3} CA^N, except that Ala224 was replaced by Glu. This substitution was originally identified as a mutation that altered HIV-1's dependence on cyclophilin A (*49*, *50*). We believe that this mutant provides a good model for the wild-type protein for three reasons. (1) It occurs in the middle of an exposed and inherently flexible 18-residue loop. (2) A related mutation

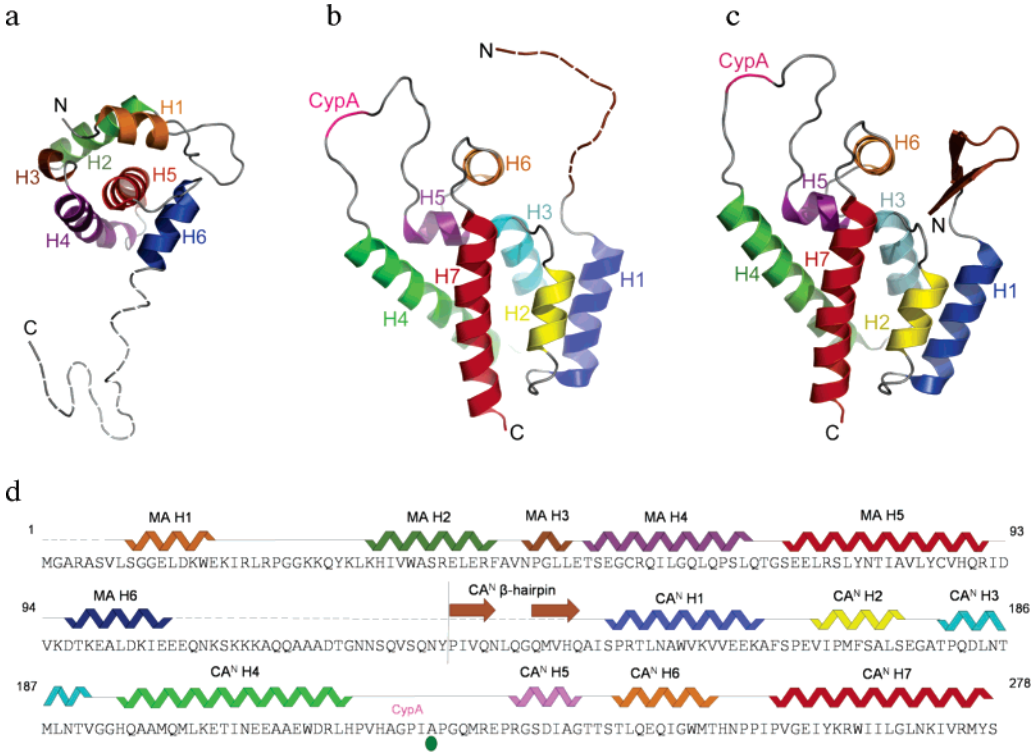

FIGURE 1: Structure of Gag_{1-278} and $CA^N_{133-278}$. (a) Cartoon representation of the Gag_{1-278} MA domain with secondary structures labeled and disordered residues shown as dashed lines. (b) Same as (a) but for the Gag_{1-278} $CA^N_{133-278}$ domain. (c) Same as (b) but for a $CA^N_{133-278}$ protein molecule. (d) Gag_{1-278} and $CA^N_{133-278}$ amino acid sequence; secondary structures above. The Gag residue numbering is used throughout the article, including that for the CA^N protein. In order to maintain consistency with earlier publications, however, we have numbered secondary structural elements separately for the MA and CA^N domains. The site of processing to separate MA and CA proteins by the viral protease is indicated with a vertical line. The β-hairpin is not formed in the Gag structure. Ala224, which is mutated to glutamate in the $CA^N_{133-278}$ construct reported here, is indicated with a dot.

(*49*) identified in the same study does not cause structural perturbation (*51*). (3) The structure superimposes closely with other available CA structures, including the preservation of the type II turn of residues 224−227. The $CA^N_{133-278}$ structure was determined by the MAD method using selenomethionine-substituted protein. The structure was refined to an *R* factor (R_{free}) of 0.205 (0.257) against 1.9 Å data and displays good geometry (Table 1). There are four CA^N molecules in the asymmetric unit.

$CA^N_{133-278}$ Structure Description. Previously reported CA^N structures that possess an authentic processed *N*-terminal sequence generally adopt a β-hairpin conformation at their *N*-termini (residues 133−145; Gag numbering). The hairpin conformation is stabilized by a salt bridge between the CA protein *N*-terminal amine and the side chain of the conserved residue Asp183 (*16*). This interaction is, therefore, not possible in the unprocessed Gag protein, which lacks the free *N*-terminal CA amine, and the conformational transition induced upon Gag processing is analogous to the mechanism of serine protease zymogen activation (*52*). Several observations indicate that the formation of the β-hairpin is important for the formation of the cone-shaped core of mature, infectious virions. For example, short extensions on the *N*-terminus of HIV-1 CA, which would block the formation of the salt bridge between the *N*-terminus and Asp183, prevented *in vitro* assembly of cylindrical assemblies that contain the same CA hexamers as those found in viral cores (*14*, *15*, *22*, *23*). Conformational assembly switches have also been reported for this region in the Gag proteins of the Mason-Pfizer monkey virus (*53*) and Rous sarcoma virus (*54*). Furthermore, mutations that blocked hairpin formation (e.g., Asp183 to Ala) resulted in the formation of noninfectious viral particles that lacked conical cores (*23*, *55*, *56*). However, although the β-hairpin structure clearly helps CA to form mature lattices *in vitro* and *in vivo*, the structure is apparently not absolutely required as recombinant CA proteins lacking the hairpin residues are capable of forming cylindrical assemblies *in vitro* that mimic the mature viral core (*23*).

Notably, just one of the four crystallographically unique molecules in our $CA^N_{133-278}$ structure displays well-defined density for the β-hairpin (Figure 1c), whereas the other three lack density for residues preceding His12 (chains A and B) or Gln13 (chain D). The failure to form β-hairpin structures is explained by the close approach of neighboring molecules in the crystal, which appears to block hairpin formation and cause the *N*-terminal 11 or 12 residues to be disordered for these three molecules. Fortuitously, the consequent availability of CA^N structures that have authentic *N*-termini and possess or lack β-hairpins provides an opportunity to estimate other conformational changes that might be coupled with hairpin formation. The overlap on Cα atoms of all 116 residues after the β-hairpin except the flexible CypA-binding loop (i.e., overlap on residues 148−216 and 232−278) gives RMSDs of 0.35−0.47 Å in pairwise overlaps of the three $CA^N_{133-278}$ molecules that lack the β-hairpin and RMSDs of 0.40−0.51 Å when these three are compared to the one that possesses the β-hairpin (Figure 2a). The largest displacement in these overlaps is for helix H1, which undergoes an apparent relative shift of ~0.7 Å in the $CA^N_{133-278}$ molecule

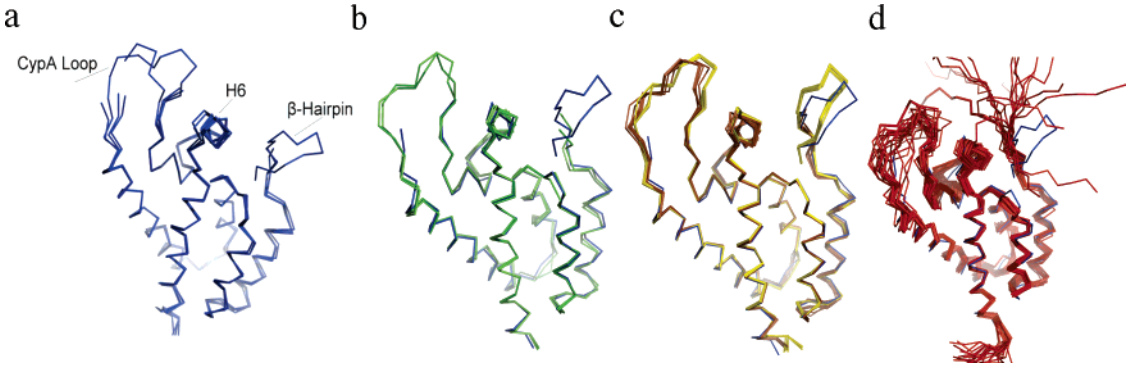

FIGURE 2: Different structures of CA^N overlap closely. (a) Cα trace of the four molecules in the $CA^N_{133-278}$ crystal asymmetric unit. Overlaps have been performed on residues 148−216 and 232−278. All subsequent panels include the one molecule shown here that possesses an ordered *N*-terminal *β*-hairpin. The CypA binding site, H6, and *β*-hairpin are indicated. (b) Including the two CA^N domains of Gag_{1-278} shown in green. (c) Including the two CA^N molecules in the asymmetric units of a series of isomorphous CypA complexes colored yellow (molecule A, possesses the *N*-terminal *β*-hairpin) or brown (molecule B, lacks the *N*-terminal *β*-hairpin). (d) Including the ensemble of CA^N domains from the Gag_{1-283} NMR structure colored red.

that possesses an *N*-terminal *β*-hairpin compared to that of the other three molecules. This displacement is evenly spaced over H1 and is not associated with a change in side-chain conformation. The structural consequences of *β*-hairpin formation appear, therefore, to be statistically significant but subtle.

The CypA-binding loop is known to be very flexible (*16*, *31*), and this is also evident in the structures reported here. Owing to different lattice contacts, one of the $CA^N_{133-278}$ molecules is ordered in this region, whereas the other three, including the molecule that adopts a *β*-hairpin, show substantial degrees of disorder and lack density for 3−6 residues in the middle of the loop.

Comparison of Gag_{1-278} and $CA^N_{133-278}$ Structures. The two CA^N domains in the Gag_{1-278} crystal asymmetric unit superimpose on each other with an RMSD of 0.57 Å on the same 116 pairs of Cα atoms for the comparisons above. They are also in close agreement with the four molecules of the $CA^N_{133-278}$ crystal structure, with RMSD values of 0.57−0.72 Å in pairwise comparisons of the 116 Cα atoms (Figure 2b). This similarity extends to previously reported crystal structures of CA^N complexes with CypA (*34*), which display RMSD values of 0.48 − 0.87 Å in equivalent overlaps (Figure 2c). These comparisons indicate that the CA^N structure is essentially unchanged upon Gag processing, *N*-terminal *β*-hairpin formation, and binding of CypA.

Lack of Large Correlated Motion between the CypA-Binding Loop, Helix6, and β-Hairpin Formation. The Gag_{1-283} NMR structure (*47*) and our Gag_{1-278} and $CA^N_{133-278}$ crystal structures are in close overall agreement; the overlap on the 116 pairs of CA^N Cα atoms gives RMSD values of 1.30−1.35 Å for the top structure in the NMR ensemble compared with our $CA^N_{133-278}$ and Gag_{1-278} crystal structures (Figure 2d). This is comparable to the agreement seen between the top NMR model and the 19 other members of the ensemble (RMSD 1.14−1.68 Å). Nevertheless, our conclusion that CA^N does not undergo significant conformational change upon processing (apart from *β*-hairpin formation) differs from the important conclusion of Tang et al. (*47*) that *β*-hairpin formation correlates with a ∼2 Å shift in CA^N helix H6 (residues 242−251). This conclusion led to the mechanistically important proposal that H6 communicates conformational information between the *β*-hairpin and CypA-binding loop and that this effect might help explain the mechanism of CypA in HIV-1 replication (*47*). Because of the importance of H6 in this analysis, Figure 3 shows unbiased electron density maps that demonstrate that our $CA^N_{133-278}$ and Gag_{1-278} models are well defined in this region.

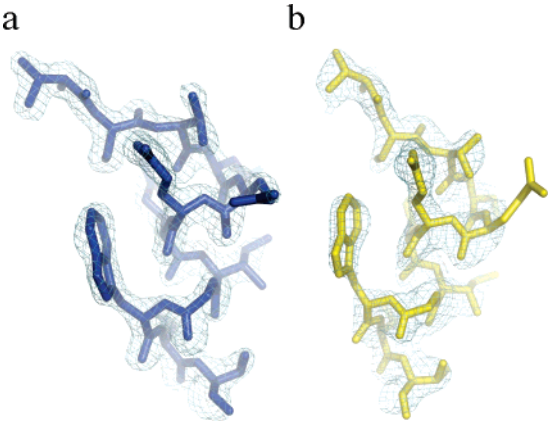

FIGURE 3: Simulated annealing omit maps (*68*) surrounding helix H6. View direction is from the top of Figure 1b and c. (a) $CA^N_{133-278}$, contoured at 1.7 × RMSD; (b) Gag_{1-278}, contoured at 1.3 × RMSD.

In order to understand the apparent differences between our observations and the conclusion of Tang et al., we performed some additional overlaps. To avoid masking potentially important shifts in the vicinity of H6, the residues included in subsequent superpositions (150−214 and 257−276) are the same as those included before but lack H6 and its flanking residues and also lack two variable residues at the *N*-terminus, two variable residues at the *C*-terminus, and H5. As shown in Figure 4, H6 adopts similar conformations in all of the available crystal structures. For example, $CA^N_{133-278}$ and Gag_{1-278} display an average displacement of H6 Cα atoms of 0.9 Å in these overlaps. The impression of little H6 displacement upon Gag processing is reinforced by consideration of two previously reported CA−Fab complexes. One of these structures has an authentic CA *N*-terminus and *β*-hairpin conformation (*57*), whereas the other retains an *N*-terminal affinity tag that prevents hairpin formation and, therefore, causes this construct to serve as a Gag mimic (*58*, *59*). H6 Cα atoms show an average displacement of 0.6 Å between these two structures, and when they are compared to $CA^N_{133-278}$ and Gag_{1-278}, the

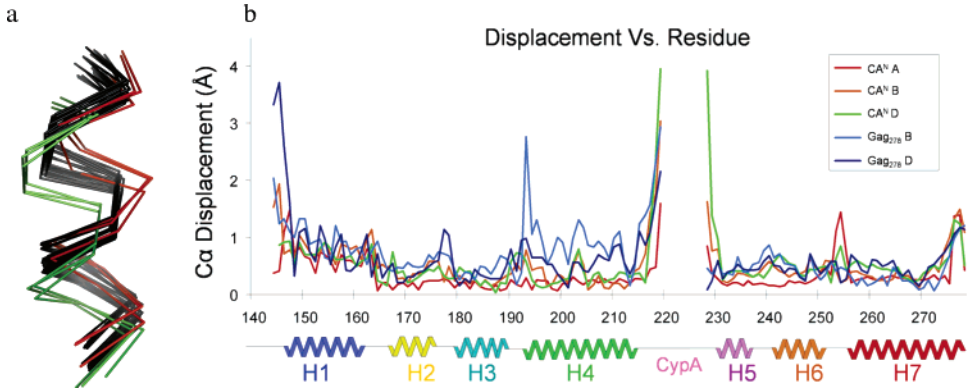

FIGURE 4: Relative motions of H6. (a) Helix H6 viewed in the same orientation as in Figure 3. Structures shown are listed in Table 3 and were overlapped on residues 150−214 and 257−276, treating the $CA^N_{133-278}$ molecule that has a β-hairpin as the reference. Crystal structures, black and NMR structures Gag_{1-283}, red and CA^N, green. (b) Displacement of Cα atoms per residue for CA^N following global overlap. The one CA^N molecule that possesses a β-hairpin is always the reference (molecule C). Overlaps with the three other CA^N molecules in the asymmetric unit, molecules A, B, and D, are colored red, orange, and green, respectively. Overlaps with the two CA^N domains in the Gag_{278} crystal structure are colored light and dark blue.

Table 3: Relative Motions of H6

			RMSD (Å)[a]	<H6> (Å)[b]	reference
black	$CA^N_{133-278}$	X-ray	0.42	0.32	this study
black	Gag_{1-278}	X-ray	0.59	0.91	this study
black	CA^N−CypA (A)	X-ray	0.49	0.95	(*34*)
black	CA^N−CypA (B)	X-ray	0.62	0.35	(*34*)
black	CA−Fab	X-ray	0.80	0.55	(*57*)
black	CA (Gag)−Fab	X-ray	0.50	0.67	(*59*)
red	Gag_{1-283}	NMR	1.29	1.69	(*47*)
green	CA^N	NMR	1.22	1.86	(*16*)

[a] Root-mean-square deviation for overlap on residues 150−214 and 257−276 against the $CA^N_{133-278}$ molecule that adopts a β-hairpin. The value given is the average overall models, for example, for the three $CA^N_{133-278}$ molecules that do not adopt a β-hairpin, a total of seven CA^N−CypA structures with a β-hairpin and seven without, and for the top three models in each of the NMR ensembles. [b] Displacement of H6 Cα atoms compared to the $CA^N_{133-278}$ molecule that adopts a β-hairpin. The value is the average over all H6 residues and all models shown.

average H6 Cα displacements are 0.6 and 0.9 Å, respectively. Furthermore, a series of 14 CA^N−CypA (*34*) complex crystal structures are in similar agreement with each other (overall RMSD ~0.45 Å; average H6 displacement ~0.55 Å) and with $CA^N_{133-278}$ (overall RMSD ~0.55 Å; average H6 displacement ~0.65 Å). Overall, these comparisons strongly indicate that H6 moves by less than 1.0 Å upon Gag processing, β-hairpin formation, and/or CypA binding and that the H6 displacements observed are comparable to the RMSD for pairwise superposition of the ordered regions of the rest of the protein (Figure 4).

The earlier conclusion that H6 moves significantly upon processing resulted from a comparison of NMR structures of CA^N (*16*) and Gag_{1-283} (*47*). Indeed, superposition of these models confirms a relative displacement of ~2.4 Å and also shows that the two NMR structures lie outside the envelope of H6 conformations seen for the various crystal structures (Figure 4a). Although the effects of crystal packing cannot be completely discounted, the large number of different crystal packing arrangements included in this analysis indicates that crystal packing is not influencing the disposition of H6. We, therefore, conclude that the displacement of H6 may not be as large as originally proposed. Close inspection of Figure 4a shows that the crystal structures do indicate a small shift of H6 in the direction described by Tang et al. upon Gag processing. For example, a comparison of the $CA^N_{133-278}$ that possesses a β-hairpin and Gag_{1-278} indicates an average displacement of 0.91 Å for H6 Cα atoms. Similarly, a comparison between the CA^N molecules in CypA complexes that either possess or lack a β-hairpin (molecules A and B in the asymmetric unit (*34*)) shows an average displacement of 0.55 Å. The direction of these H6 displacements between CA^N crystals structures that lack or possess β-hairpins corresponds to the direction seen in the overlap performed by Tang et al. (*47*), although their magnitudes are smaller.

H6 does not appear to be especially mobile in the crystal structures. In Gag_{1-278} and $CA^N_{133-278}$, H6 B values (Cα atoms) are close to the average for all ordered regions in these structures. H6 B values are also close to average for about half of the CA^N−CypA complexes (*34*), and are only slightly elevated, typically ~40 $Å^2$ compared to ~30 $Å^2$ for other helices, in the remaining CA^N−CypA complexes. Thus, H6 appears to be only slightly more mobile than other parts of the structure. This impression is reinforced by comparison of displacements on a per residue basis after global overlap (Figure 4b).

Because H6 lies between the *N*-terminal β-hairpin and the CypA-binding loop, Tang et al. proposed that the apparent movement of H6 upon β-hairpin formation was correlated with CypA binding (*47*). Further, Bristow et al. reported ELISA data that indicated that the affinity of CypA for Gag is 1000-fold greater than its affinity for the mature CA protein (*60*). It was, therefore, suggested that correlation between CypA binding and β-hairpin formation might underlie the role of CypA in HIV-1 infectivity (*47*). The ELISA data conflict, however, with our earlier surface plasmon resonance study that found no significant difference in CypA affinity for CA ($Kd = 15$ (*5*) μM) and MA-CA/Gag_{1-363} ($Kd = 12$ (*1*) μM) constructs (*32*). They also conflict with NMR data indicating that CypA binding and catalysis are the same for CA, CA^N, and MA−CA^N constructs (*61*). Furthermore, early models indicated that CypA was packaged into the virion and then participated in early steps in viral replication in the new target cell (*30*, *62*, *63*), which made potential correlation with β-hairpin formation an attractive possibility. Currently, however, the leading model is that CypA binds

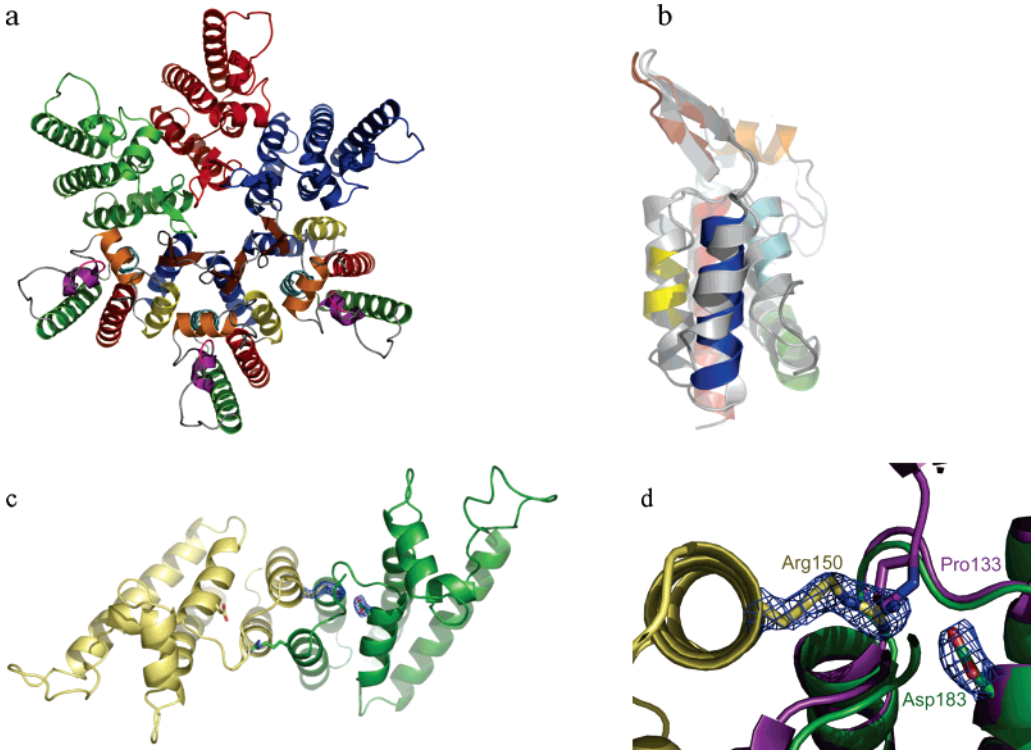

FIGURE 5: CA^N assembly. (a) Model of the HIV-1 CA^N hexamer obtained by overlapping $CA^N_{133-278}$ subunits onto the MLV CA^N crystal structure (*18*). The three subunits at the top of the Figure have solid colors (green, red, and blue). The three lower subunits are colored by secondary structure, using the same color scheme as that in Figure 1c. (b) Single subunits of MLV CA^N (gray) and superimposed HIV-1 CA^N (secondary structure coloring), viewed from the center of the hexamer model. (c) Two-fold symmetric packing of the two CA^N domains (tan and green) in the Gag_{1-278} asymmetric unit. Arg150 of one CA^N binds Asp183 of its neighbor. A simulated annealing omit map is shown around one Arg150−Asp183 pair. A similar but slightly more open structure is seen for the other Arg150−Asp183 interaction. (d) Close-up view of panel (c). The Arg150 side chain would clash with the *N*-terminal Pro133 in the mature conformation (purple).

CA in the target cell and modulates interactions with host restriction factors (*25*−*29*). For these reasons, we conclude that movements in H6 are unlikely to substantially affect CypA interactions in coordination with β-hairpin formation.

The Gag_{1-283} NMR data showed doubling of a set of peaks for H6 residues Glu177 and Gly178, which appeared to indicate slow exchange between two local conformations that differ in phi/psi angles for residues 177−179 (*47*). An inspection of the top 20 structures from this ensemble does not reveal obvious alternative conformations for all these residues, although the peptide bond between residues 176 and 177 is found in two distinctly different orientations that are approximately 180° flipped with respect to each other. In contrast, the various crystal structures only show a single conformation for these residues.

Implications for Core Assembly. The question remains as to how the formation of the β-hairpin promotes viral maturation and infectivity. A possible role was suggested from the structure of MLV CA^N (*18*). This protein shares negligible sequence identity with HIV-1 CA^N, yet adopts a similar tertiary structure (RMSD = 2.9 Å for overlap of 85 Cα atoms). Importantly, the MLV CA^N formed a hexameric arrangement in the crystal that appears to mimic the organization within viral cores inferred from electron microscopic analysis of assembled CA proteins *in vitro* (*13*, *14*, *64*, *65*) and in viral cores (*15*, *66*). We have docked our HIV $CA^N_{133-278}$ structure onto the MLV CA^N structure to develop a model of the HIV-1 CA^N hexamer (Figure 5). This modeling is consistent with earlier conclusions that subunit interactions within the hexamer are mediated by residues of helices H1, H2, and H3 (*18*). It was also suggested that the six *N*-terminal β-hairpins might stabilize hexamerization by interacting with each other, although this possibility is not strongly supported by the MLV CA^N structure or the corresponding HIV-1 CA^N model because hairpins from adjacent subunits do not make extensive direct contacts (*18*). Another possibility is that formation of the β-hairpin might stabilize CA^N hexamers indirectly by stabilizing the appropriate conformation of residues such as Pro149, which mediate subunit contacts at the *C*-terminal end of the β-hairpin or the *N*-terminal end of H1 (*18*). Another possibility, suggested by the observation that H1 undergoes an ~0.7 Å apparent displacement between $CA^N_{133-278}$ and Gag_{1-278} crystal structures, is that β-hairpin formation stabilizes the appropriate arrangement of helices that mediate subunit contacts. Unfortunately, this analysis is limited by the low similarity of sequence and structural detail between MLV and HIV CA^N proteins. Overall, our analysis suggests that beyond β-hairpin formation, the structural effects of Gag processing are subtle. This is consistent with the inherently weak and cooperative hexamerization of CA^N and the consequent amplification that would allow small energy changes to drive the equilibrium.

A speculative possibility suggested by the crystal structures is that β-hairpin formation might act, in part, to displace an interaction that stabilizes the immature Gag lattice. This model would explain why CA proteins lacking the hairpin residues are capable of forming cylindrical in vitro assemblies that mimic the packing of mature viral capsids (*23*). As shown in Figure 5c and d, the two CA^N domains of the

Gag_{1-278} asymmetric unit pack with approximate 2-fold symmetry, with the guanidinium of CA^N Arg150 binding the neighboring CA^N domain in the same place as the *N*-terminal amine (Pro133) of the mature CA^N molecule. A possible importance of this interaction is suggested by the high conservation seen for Arg150, which is highly surface exposed in the monomer. Moreover, because this interaction is incompatible with formation of the β-hairpin, the processing of Gag by the viral protease may trigger the structural rearrangements of maturation by a combination of allowing new interactions and displacing interactions that stabilize the immature lattice. Resolution of these models will require further study.

ACKNOWLEDGMENT

We thank Michael Summers for critical comments on the manuscript. The use of the National Synchrotron Light Source, Brookhaven National Laboratory, was supported by the U.S. Department of Energy, Office of Science, Office of Basic Energy Sciences, under Contract No. DE-AC02-98CH10886. Portions of this research were carried out at the Stanford Synchrotron Radiation Laboratory, a national user facility operated by Stanford University on behalf of the U.S. Department of Energy, Office of Basic Energy Sciences. The SSRL Structural Molecular Biology Program is supported by the Department of Energy, Office of Biological and Environmental Research, and by the National Institutes of Health, National Center for Research Resources, Biomedical Technology Program, and the National Institute of General Medical Sciences.

REFERENCES

1. Briggs, J. A., Simon, M. N., Gross, I., Krausslich, H. G., Fuller, S. D., Vogt, V. M., and Johnson, M. C. (2004) The stoichiometry of Gag protein in HIV-1, *Nat. Struct. Mol. Biol. 11*, 672−675.
2. Frankel, A. D., and Young, J. A. (1998) HIV-1: fifteen proteins and an RNA, *Annu. Rev. Biochem. 67*, 1−25.
3. Göttlinger, H. (2001) in *HIV Sequence Compendium 2001* (Kuiken, C., Foley, B., Hahn, B., Marx, P., McCutchan, F., Mellors, J. W., Wolinsky, S., and Korber, B., Eds.) pp 2−28, Theoretical Biology and Biophysics Group, Los Alamos National Laboratory, Los Alamos, NM, LA-UR 02-2877.
4. Zhou, W., Parent, L. J., Wills, J. W., and Resh, M. D. (1994) Identification of a membrane-binding domain within the amino-terminal region of human immunodeficiency virus type 1 Gag protein which interacts with acidic phospholipids, *J. Virol. 68*, 2556−2569.
5. Massiah, M. A., Starich, M. R., Paschall, C., Summers, M. F., Christensen, A. M., and Sundquist, W. I. (1994) Three-dimensional structure of the human immunodeficiency virus type 1 matrix protein, *J. Mol. Biol. 244*, 198−223.
6. Tang, C., Loeliger, E., Luncsford, P., Kinde, I., Beckett, D., and Summers, M. F. (2004) Entropic switch regulates myristate exposure in the HIV-1 matrix protein, *Proc. Natl. Acad. Sci. U.S.A. 101*, 517−522.
7. Hill, C. P., Worthylake, D., Bancroft, D. P., Christensen, A. M., and Sundquist, W. I. (1996) Crystal structures of the trimeric human immunodeficiency virus type 1 matrix protein: implications for membrane association and assembly, *Proc. Natl. Acad. Sci. U.S.A. 93*, 3099−3104.
8. Rao, Z., Belyaev, A. S., Fry, E., Roy, P., Jones, I. M., and Stuart, D. I. (1995) Crystal structure of SIV matrix antigen and implications for virus assembly, *Nature 378*, 743−747.
9. Cosson, P. (1996) Direct interaction between the envelope and matrix proteins of HIV-1, *EMBO J. 15*, 5783−5788.
10. Murakami, T., and Freed, E. O. (2000) Genetic evidence for an interaction between human immunodeficiency virus type 1 matrix and alpha-helix 2 of the gp41 cytoplasmic tail, *J. Virol. 74*, 3548−3554.
11. Fuller, S. D., Wilk, T., Gowen, B. E., Krausslich, H. G., and Vogt, V. M. (1997) Cryo-electron microscopy reveals ordered domains in the immature HIV-1 particle, *Curr. Biol. 7*, 729−738.
12. Wilk, T., Gross, I., Gowen, B. E., Rutten, T., de Haas, F., Welker, R., Krausslich, H. G., Boulanger, P., and Fuller, S. D. (2001) Organization of immature human immunodeficiency virus type 1, *J. Virol. 75*, 759−771.
13. Ganser, B. K., Li, S., Klishko, V. Y., Finch, J. T., and Sundquist, W. I. (1999) Assembly and analysis of conical models for the HIV-1 core, *Science 283*, 80−83.
14. Li, S., Hill, C. P., Sundquist, W. I., and Finch, J. T. (2000) Image reconstructions of helical assemblies of the HIV-1 CA protein, *Nature 407*, 409−413.
15. Briggs, J. A., Wilk, T., Welker, R., Krausslich, H. G., and Fuller, S. D. (2003) Structural organization of authentic, mature HIV-1 virions and cores, *Embo J. 22*, 1707−1715.
16. Gitti, R. K., Lee, B. M., Walker, J., Summers, M. F., Yoo, S., and Sundquist, W. I. (1996) Structure of the amino-terminal core domain of the HIV-1 capsid protein, *Science 273*, 231−235.
17. Gamble, T. R., Yoo, S., Vajdos, F. F., von Schwedler, U. K., Worthylake, D. K., Wang, H., McCutcheon, J. P., Sundquist, W. I., and Hill, C. P. (1997) Structure of the carboxyl-terminal dimerization domain of the HIV-1 capsid protein, *Science 278*, 849−853.
18. Mortuza, G. B., Haire, L. F., Stevens, A., Smerdon, S. J., Stoye, J. P., and Taylor, I. A. (2004) High-resolution structure of a retroviral capsid hexameric amino-terminal domain, *Nature 431*, 481−485.
19. Worthylake, D. K., Wang, H., Yoo, S., Sundquist, W. I., and Hill, C. P. (1999) Structures of the HIV-1 capsid protein dimerization domain at 2.6 A resolution, *Acta Crystallogr., Sect. D. 55*, 85−92.
20. Ivanov, D., Stone, J. R., Maki, J. L., Collins, T., and Wagner, G. (2005) Mammalian SCAN domain dimer is a domain-swapped homolog of the HIV capsid C-terminal domain, *Mol. Cell 17*, 137−143.
21. Lanman, J., Lam, T. T., Emmett, M. R., Marshall, A. G., Sakalian, M., and Prevelige, P. E., Jr. (2004) Key interactions in HIV-1 maturation identified by hydrogen-deuterium exchange, *Nat. Struct. Mol. Biol. 11*, 676−677.
22. Gross, I., Hohenberg, H., Huckhagel, C., and Krausslich, H. G. (1998) N-Terminal extension of human immunodeficiency virus capsid protein converts the in vitro assembly phenotype from tubular to spherical particles, *J. Virol. 72*, 4798−4810.
23. von Schwedler, U. K., Stemmler, T. L., Klishko, V. Y., Li, S., Albertine, K. H., Davis, D. R., and Sundquist, W. I. (1998) Proteolytic refolding of the HIV-1 capsid protein amino-terminus facilitates viral core assembly, *EMBO J. 17*, 1555−1568.
24. Goff, S. P. (2004) Genetic control of retrovirus susceptibility in mammalian cells, *Annu. Rev. Genet. 38*, 61−85.
25. Sokolskaja, E., Sayah, D. M., and Luban, J. (2004) Target cell cyclophilin A modulates human immunodeficiency virus type 1 infectivity, *J. Virol. 78*, 12800−12808.
26. Towers, G. J., Hatziioannou, T., Cowan, S., Goff, S. P., Luban, J., and Bieniasz, P. D. (2003) Cyclophilin A modulates the sensitivity of HIV-1 to host restriction factors, *Nat. Med. 9*, 1138−1143.
27. Owens, C. M., Song, B., Perron, M. J., Yang, P. C., Stremlau, M., and Sodroski, J. (2004) Binding and susceptibility to postentry restriction factors in monkey cells are specified by distinct regions of the human immunodeficiency virus type 1 capsid, *J. Virol. 78*, 5423−5437.
28. Hatziioannou, T., Perez-Caballero, D., Cowan, S., and Bieniasz, P. D. (2005) Cyclophilin interactions with incoming human immunodeficiency virus type 1 capsids with opposing effects on infectivity in human cells, *J. Virol. 79*, 176−183.
29. Berthoux, L., Sebastian, S., Sokolskaja, E., and Luban, J. (2005) Cyclophilin A is required for TRIM5{alpha}-mediated resistance to HIV-1 in Old World monkey cells, *Proc. Natl. Acad. Sci. U.S.A. 102*, 14849−14853.
30. Franke, E. K., Yuan, H. E., and Luban, J. (1994) Specific incorporation of cyclophilin A into HIV-1 virions, *Nature 372*, 359−362.
31. Gamble, T. R., Vajdos, F. F., Yoo, S., Worthylake, D. K., Houseweart, M., Sundquist, W. I., and Hill, C. P. (1996) Crystal structure of human cyclophilin A bound to the amino-terminal domain of HIV-1 capsid, *Cell 87*, 1285−1294.

32. Yoo, S., Myszka, D. G., Yeh, C., McMurray, M., Hill, C. P., and Sundquist, W. I. (1997) Molecular recognition in the HIV-1 capsid/cyclophilin A complex, *J. Mol. Biol. 269*, 780−795.
33. Bosco, D. A., Eisenmesser, E. Z., Pochapsky, S., Sundquist, W. I., and Kern, D. (2002) Catalysis of cis/trans isomerization in native HIV-1 capsid by human cyclophilin A, *Proc. Natl. Acad. Sci. U.S.A. 99*, 5247−5252.
34. Howard, B. R., Vajdos, F. F., Li, S., Sundquist, W. I., and Hill, C. P. (2003) Structural insights into the catalytic mechanism of cyclophilin A, *Nat. Struct. Biol. 10*, 475−481.
35. Eisenmesser, E. Z., Bosco, D. A., Akke, M., and Kern, D. (2002) Enzyme dynamics during catalysis, *Science 295*, 1520−1523.
36. Studier, F. W., and Moffatt, B. A. (1986) Use of bacteriophage T7 RNA polymerase to direct selective high-level expression of cloned genes, *J. Mol. Biol. 189*, 113−130.
37. Otwinowski, Z., and Minor, W. (1997) Processing of X-ray diffraction data collected in oscillation mode, *Methods Enzymol. 276*, 307−326.
38. Terwilliger, T. (2004) SOLVE and RESOLVE: automated structure solution, density modification and model building, *J. Synchrotron Radiat. 11*, 49−52.
39. Jones, T. A., Zou, J. Y., Cowan, S. W., and Kjeldgaard, M. (1991) Improved methods for building protein models in electron density maps and the location of errors in these models, *Acta Crystallogr., Sect. A 47*, 110−119.
40. Murshudov, G. N. (1997) Refinement of macromolecular structures by the maximum-likelihood method, *Acta Crystallogr., Sect. D 53*, 240−255.
41. Van Duyne, G. D., Standaert, R. F., Karplus, P. A., Schreiber, S. L., and Clardy, J. (1993) Atomic structures of the human immunophilin FKBP-12 complexes with FK506 and rapamycin, *J. Mol. Biol. 229*, 105−124.
42. Terwilliger, T. C., and Berendzen, J. (1999) Automated structure solution for MIR and MAD, *Acta Crystallogr., Sect. D 55*, 849−861.
43. Kissinger, C. R., Gehlhaar, D. K., and Fogel, D. B. (1999) Rapid automated molecular replacement by evolutionary search, *Acta Crystallogr., Sect. D 55*, 484−491.
44. Collaborative computational project, N. (1994) The CCP4 suite: programs for protein crystallography, *Acta Crystallogr., Sect. D 50*, 760−763.
45. McRee, D. E. (1999) XtalView/Xfit−A versatile program for manipulating atomic coordinates and electron density, *J. Struct. Biol. 125*, 156−165.
46. DeLano, W. L. (2002), DeLano Scientific, San Carlos, CA.
47. Tang, C., Ndassa, Y., and Summers, M. F. (2002) Structure of the N-terminal 283-residue fragment of the immature HIV-1 Gag polyprotein, *Nat. Struct. Biol. 9*, 537−543.
48. Massiah, M. A., Worthylake, D., Christensen, A. M., Sundquist, W. I., Hill, C. P., and Summers, M. F. (1996) Comparison of the NMR and X-ray structures of the HIV-1 matrix protein: evidence for conformational changes during viral assembly, *Protein Sci. 5*, 2391−2398.
49. Aberham, C., Weber, S., and Phares, W. (1996) Spontaneous mutations in the human immunodeficiency virus type 1 gag gene that affect viral replication in the presence of cyclosporins, *J. Virol. 70*, 3536−3544.
50. Braaten, D., Aberham, C., Franke, E. K., Yin, L., Phares, W., and Luban, J. (1996) Cyclosporine A-resistant human immunodeficiency virus type 1 mutants demonstrate that Gag encodes the functional target of cyclophilin A, *J. Virol. 70*, 5170−5176.
51. Campos-Olivas, R., and Summers, M. F. (1999) Backbone dynamics of the N-terminal domain of the HIV-1 capsid protein and comparison with the G94D mutant conferring cyclosporin resistance/dependence, *Biochemistry 38*, 10262−10271.
52. Sigler, P. B., Blow, D. M., Matthews, B. W., and Henderson, R. (1968) Structure of crystalline -chymotrypsin. II. A preliminary report including a hypothesis for the activation mechanism, *J. Mol. Biol. 35*, 143−164.
53. Rumlova-Klikova, M., Hunter, E., Nermut, M. V., Pichova, I., and Ruml, T. (2000) Analysis of Mason-Pfizer monkey virus Gag domains required for capsid assembly in bacteria: role of the N-terminal proline residue of CA in directing particle shape, *J. Virol. 74*, 8452−8459.
54. Nandhagopal, N., Simpson, A. A., Johnson, M. C., Francisco, A. B., Schatz, G. W., Rossmann, M. G., and Vogt, V. M. (2004) Dimeric rous sarcoma virus capsid protein structure relevant to immature Gag assembly, *J. Mol. Biol. 335*, 275−282.
55. Tang, S., Murakami, T., Agresta, B. E., Campbell, S., Freed, E. O., and Levin, J. G. (2001) Human immunodeficiency virus type 1 N-terminal capsid mutants that exhibit aberrant core morphology and are blocked in initiation of reverse transcription in infected cells, *J. Virol. 75*, 9357−9366.
56. Rue, S. M., Roos, J. W., Amzel, L. M., Clements, J. E., and Barber, S. A. (2003) Hydrogen bonding at a conserved threonine in lentivirus capsid is required for virus replication, *J. Virol. 77*, 8009−8018.
57. Momany, C., Kovari, L. C., Prongay, A. J., Keller, W., Gitti, R. K., Lee, B. M., Gorbalenya, A. E., Tong, L., McClure, J., Ehrlich, L. S., Summers, M. F., Carter, C., and Rossmann, M. G. (1996) Crystal structure of dimeric HIV-1 capsid protein, *Nat. Struct. Biol. 3*, 763−770.
58. Berthet-Colominas, C., Monaco, S., Novelli, A., Sibai, G., Mallet, F., and Cusack, S. (1999) Head-to-tail dimers and interdomain flexibility revealed by the crystal structure of HIV-1 capsid protein (p24) complexed with a monoclonal antibody Fab, *EMBO J. 18*, 1124−1136.
59. Monaco-Malbet, S., Berthet-Colominas, C., Novelli, A., Battai, N., Piga, N., Cheynet, V., Mallet, F., and Cusack, S. (2000) Mutual conformational adaptations in antigen and antibody upon complex formation between an Fab and HIV-1 capsid protein p24, *Structure Fold Des. 8*, 1069−1077.
60. Bristow, R., Byrne, J., Squirell, J., Trencher, H., Carter, T., Rodgers, B., Saman, E., and Duncan, J. (1999) Human cyclophilin has a significantly higher affinity for HIV-1 recombinant p55 than p24, *J. Acquired Immune Defic Syndr. Hum. Retrovirol. 20*, 334−336.
61. Bosco, D. A., and Kern, D. (2004) Catalysis and binding of cyclophilin A with different HIV-1 capsid constructs, *Biochemistry 43*, 6110−6119.
62. Braaten, D., Franke, E. K., and Luban, J. (1996) Cyclophilin A is required for an early step in the life cycle of human immunodeficiency virus type 1 before the initiation of reverse transcription, *J. Virol. 70*, 3551−3560.
63. Thali, M., Bukovsky, A., Kondo, E., Rosenwirth, B., Walsh, C. T., Sodroski, J., and Gottlinger, H. G. (1994) Functional association of cyclophilin A with HIV-1 virions, *Nature 372*, 363−365.
64. Ganser, B. K., Cheng, A., Sundquist, W. I., and Yeager, M. (2003) Three-dimensional structure of the M-MuLV CA protein on a lipid monolayer: a general model for retroviral capsid assembly, *EMBO J. 22*, 2886−2892.
65. Mayo, K., Vana, M. L., McDermott, J., Huseby, D., Leis, J., and Barklis, E. (2002) Analysis of Rous sarcoma virus capsid protein variants assembled on lipid monolayers, *J. Mol. Biol. 316*, 667−678.
66. Benjamin, J., Ganser-Pornillos, B. K., Tivol, W. F., Sundquist, W. I., and Jensen, G. J. (2005) Three-dimensional structure of HIV-1 virus-like particles by electron cryotomography, *J. Mol. Biol. 346*, 577−588.
67. Laskowski, R. A., MacArthur, M. W., Moss, D. S., and Thornton, J. M. (1993) PROCHECK: a program to check the stereochemical quality of protein structures, *J. Appl. Crystallogr. 26*, 283−291.
68. Hodel, A., Kim, S.-H., and Brünger, A. T. (1992) Model bias in macromolecular crystal structures, *Acta Crysallogr., Sect. A 48*, 851−858.

BI060927X